Extraction of Dielectric Constant and Loss Tangent Using New Rapid Plane Solver and Analytical Debye Modeling for Printed Circuit Boards

A. Ege Engin, *Member, IEEE*

***Abstract*—Dielectric material properties of printed circuit boards (PCBs) are needed by designers working in various areas such as signal integrity, antennas, and embedded RF components. Among many methods to extract the material properties, the full sheet resonance technique is commonly used on PCBs due to its simplicity. The disadvantage of this method is that an analytical equation is used to extract the dielectric constant, which is accurate only for lossless dielectrics. In this paper, a new method is presented to solve the inaccuracy issue of the extraction of the dielectric constant by applying customized electromagnetic simulation based on a new rapid plane solver instead of analytical equations. For PCB dielectrics, the loss tangent tends to be flat over several decades. The dielectric constant then varies as a function of frequency based on the Kronig–Kramers relations. This paper introduces a new Debye type of a model for the complex permittivity of such dielectrics. The parameters of the Debye model can be obtained analytically without requiring any curve fitting. The resulting Debye model can then be easily integrated in SPICE or a finite-difference time-domain simulator.**

***Index Terms*—Causality, complex permittivity, debye, dielectric constant, flat sheet resonance, loss tangent, rapid solver, vector fitting.**

I. Introduction

ACCURATE estimation of the dielectric constant and loss tangent at high frequencies is becoming increasingly important as the frequency content of the signals in printed circuit boards (PCBs) and chip packages increase. Accuracy of the design of embedded RF components and planar antennas on PCBs depend highly on the knowledge of the dielectric material properties. The signal integrity of a high-speed link can also suffer from closed eye diagrams due to dielectric losses. Although low-loss dielectrics are available to achieve high-Q RF compenents and improved signal integrity, they come at a higher cost. Accurate estimation of the broadband dielectric constant and loss tangent as a function of frequency is, therefore, critical.

Many techniques are available to characterize the material properties, such as the short-pulse propagation technique based on time-domain reflectometry measurements [1], microstrip bandpass filters [2], or microstrip gap or ring resonators [3]–[5].

Manuscript received May 26, 2009; revised October 13, 2009. First published December 11, 2009; current version published January 13, 2010.

The author is with the Department of Electrical and Computer Engineering, San Diego State University, San Diego, CA 92182 USA (e-mail: aengin@mail.sdsu.edu).

Color versions of one or more of the figures in this paper are available online at http://ieeexplore.ieee.org.

Digital Object Identifier 10.1109/TMTT.2009.2036338

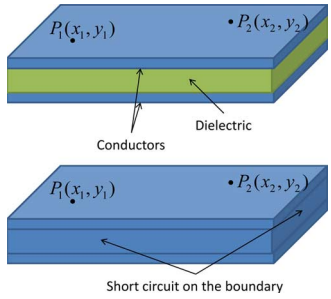

Fig. 1. Test structures used in the full sheet resonance technique. (*top*) With open boundaries. (*bottom*) With shorted boundaries.

A survey of commonly used techniques for characterization of PCB dielectrics is provided in [6].

A simple method for dielectric material characterization is the full sheet resonance method [7]–[10]. In this technique, and in its variations, a parallel-plate waveguide resonator, as shown in Fig. 1 (*top*) with open boundaries, is used. Typically a two-port measurement is performed, where the locations of the two ports P_1 and P_2 can be defined for convenience of measurement or based on the waveguide resonator modes to be excited. The two-port measurement is preferred since it helps to deembed the probe inductance automatically out of the measurements of transfer impedance. A similar waveguide resonator with shorted boundaries, as in Fig. 1 (*bottom*), could also be used with the advantage of eliminating radiation losses and fringe effect [11]. A large number of vias should be used in the shorted waveguide resonator in order to reduce the inductance of the vias and obtain an accurate electric wall boundary.

In the classical full sheet resonance method [7], an analytical equation is used to estimate the dielectric constant at resonance frequencies of the open resonator as

$$\varepsilon = \frac{1}{4{f_c}^2 \mu}\left[\left(\frac{m}{a}\right)^2 + \left(\frac{n}{b}\right)^2\right] \tag{1}$$

at the discrete resonance frequency f_c of the TM_{mn0} mode of the waveguide resonator. This equation is accurate for negligible conductor losses; hence, it becomes inaccurate at higher frequencies. The resonance frequency also changes depending on the location of the probes (P_1 and P_2) [9]. The loss tangent is then extracted from the quality factor of the waveguide resonator. However, this requires accurate knowledge of the conductor losses and radiation losses. In [10], electromagnetic (EM) simulation of the measured resonator has been used to compensate for these effects, except for the radiation losses.

In this paper, the shorted resonator is compared against the commonly used open resonator using full-wave EM simulation, as well as a new rapid plane solver that speeds up the computation time significantly. The rapid plane solver is based on the fast Poisson solver described in [12]. In the presented approach, dielectric material properties are extracted by overlapping simulation results with measured results. As such, this new method does not suffer from the inaccuracies of the standard full-sheet resonance method in extraction of dielectric constant or loss tangent. The method is applied to extract the dielectric constant and loss tangent of a low-loss and a standard FR-4 substrate. The presented approach is different than [10], as a shorted resonator is used instead of an open resonator. This paper also presents a new method for time-domain modeling of complex permittivity.

After the dielectric constant and loss tangent have been extracted at resonance frequencies, a Debye model can be constructed to interpolate and use the data in circuit or finite-difference time-domain (FDTD) simulators. On the other hand, obtaining the parameters of the Debye model using standard curve-fitting approaches is difficult, as the additional constraints of passivity and *RC* type of a circuit topology need to be enforced. Most PCB dielectrics, however, have an approximately constant loss tangent over the frequency ranges of interest, whereas the dielectric constant decreases with frequency. For such dielectrics, a closed-form expression exist, which is an irrational function. In this paper, a passive *RC* network realization, which corresponds to a Debye model, of such an irrational function is presented. This allows the determination of the parameters of the Debye model analytically using simple equations without requiring any curve fitting.

The main contributions of this paper can be summarized as follows.

1) A numerical algorithm called a "rapid plane solver" is applied for the first time for EM characterization of shorted waveguide resonators. The application of the numerical method instead of the analytical equation in (1) improves the accuracy of the extracted dielectric constant.
2) Optimum placement of probe locations is investigated.
3) The rapid plane solver is applied to extract the dielectric constant and loss tangent of a low-loss dielectric and FR-4 using shorted resonators.
4) A methodology is presented to obtain the parameters of a Debye model analytically. The result is the realization of a time-domain model representing frequency-dependent complex permittivity.

II. Rapid Plane Solver

In this section, a new numerical method is presented to obtain the impedance matrix of the shorted waveguide resonator in Fig. 1. Using a numerical method improves the accuracy of predicting the resonance frequency of the structure for lossy conductors and dielectrics compared to the analytical equation in (1), which is accurate only for lossless dielectrics.

Instead of applying a general full-wave EM simulator, we make use of the fact that the thickness of the dielectric is much smaller than the lateral dimensions; hence, the variation of the electric and magnetic fields with respect to the z-direction can be neglected. This assumption is also the basis of the analytical equation in (1). The voltage $u(x,y)$ at any point $P(x,y)$ can then be described with the 2-D Helmholtz wave equation

$$\nabla^2 u + k^2 u = -jJ_z \omega \mu d. \tag{2}$$

A. Shorted Resonator

For the shorted resonator type, the boundary conditions are of Dirichlet type, $u = 0$, along the boundaries of the resonator. One way to solve this equation numerically is by using the finite-difference method (FDM). The five-point discretization of the Laplace operator (∇^2) results in a linear equation system that can be expressed as

$$\begin{bmatrix} T & -E & 0 & 0 \\ -E & T & -E & 0 \\ 0 & \ddots & \ddots & \ddots \\ 0 & 0 & -E & T \end{bmatrix} \begin{bmatrix} V \end{bmatrix} = j\omega\mu d \begin{bmatrix} I \end{bmatrix} \tag{3}$$

where V is a vector of voltages on a rectangular grid. The nodes are numbered using canonical ordering of interior points, i.e., starting from left to right and then bottom to top. The vector I represents any current sources connected between the two plates. The system matrix has a block-diagonal shape, with the matrices T in the center and off-diagonal blocks as identity matrices E of size $(N_1 - 1) \times (N_1 - 1)$, where N_1 is the number of discretized segments in the direction from left to right. The submatrix T has the structure

$$T = \begin{bmatrix} 4 - h^2k^2 & -1 & 0 & 0 \\ -1 & 4 - h^2k^2 & -1 & 0 \\ 0 & \ddots & \ddots & \ddots \\ 0 & 0 & -1 & 4 - h^2k^2 \end{bmatrix}. \tag{4}$$

In general, this type of a linear equation system can be efficiently solved using a sparse algorithm based on nested dissection. However, a much more efficient solver can be obtained by considering the special structure of T, as it can be diagonalized using the discrete sine transform. This property can be used to transform the system matrix into a tridiagonal matrix, to speed up the computation compared to a general-purpose sparse matrix solver [12].

Fig. 2 shows the simulation results for a square-shaped shorted resonator that is excited at the center at 1 GHz. The resonator has lateral dimensions of 1 m × 1 m and a separation between the two plates of 200 μm. The permittivity and permeability of free space has been used in these simulations and losses have not been included. In the rapid solver, the structure has been descritized using 64 segments on each direction (i.e., $N_1 = 64$), which resulted in 3969 unknowns. To validate the results, the finite-element method (FEM) has been applied on the same problem. In the FEM, 2705 nodes were used. Slight differences between the simulation results can be seen. First, in displaying the results from the rapid solver, the voltage at the boundaries has not been shown in the figure since they are eliminated while setting up the matrix system in (3). Second, there is a slight asymmetry in FEM results (although the simulation setup is symmetric) since the point source in the center is actually distributed along the three nodes of the triangle in the center, causing a slight asymmetry. In the rapid solver, a perfect

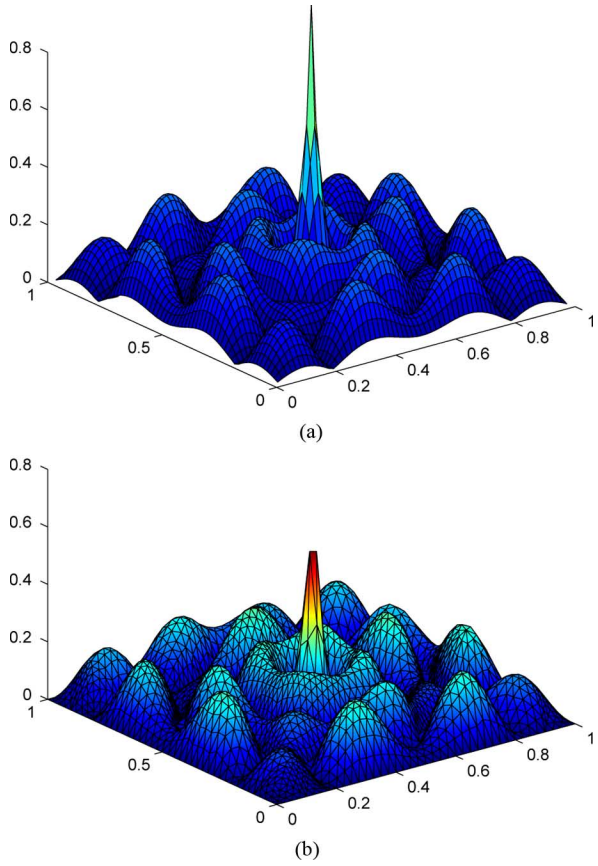

Fig. 2. Simulation mesh and voltage distribution on a square-shaped (1 m on a side) shorted resonator. (a) Using a rapid solver with $N_1 = 64$. (b) Using the FEM.

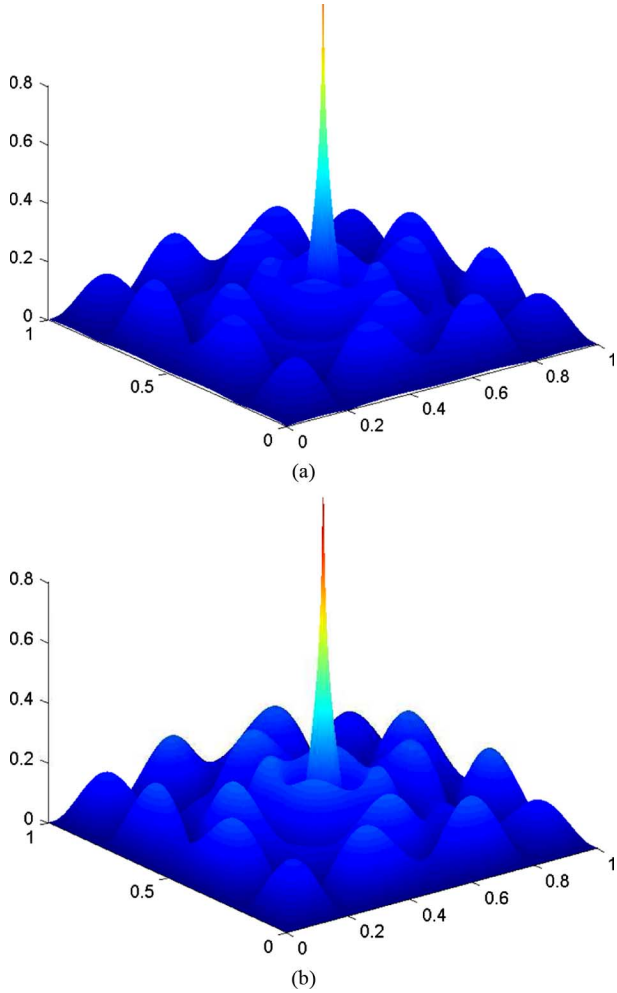

Fig. 3. Voltage distribution on a square-shaped (1 m on a side) shorted resonator. (a) Using a rapid solver with $N_1 = 512$. (b) Using the FEM.

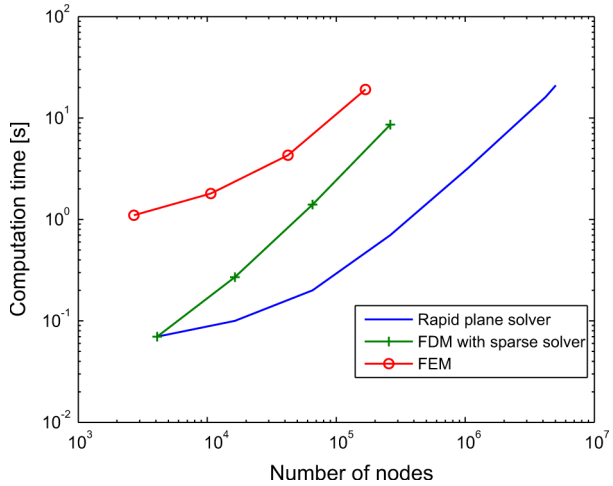

Fig. 4. Simulation time in seconds for three different numerical techniques investigated.

symmetry can be observed. To see whether these differences vanish for increased mesh density, further simulations were done. Fig. 3 shows the simulation results with a mesh size of $N_1 = 512$ for the rapid solver, and about 160-K nodes for the FEM case. It can be seen that the two results have converged to each other, except at the singular point of the excitation point source in the center.

Since the FEM uses a different mesh than the rapid solver, a slight deviation is expected. However, a direct solution of the matrix in (3) should provide a result within round-off error to the rapid solver result. This has been confirmed through simulations as well. Since the results of the direct FDM solver is essentially the same as for the rapid solver, they are not reproduced here. As for the run times, Fig. 4 provides a comparison of the three different methods investigated. The rapid plane solver can be used to simulate shorted resonators with as many as five million nodes, whereas a standard FEM or FDM code runs out of memory for less than a million nodes. The simulations were done on a laptop PC with 3 GB of RAM and a clock frequency of 1.4 GHz. For similar number of nodes, the speed-up obtained in using the rapid planes solver compared to the (2-D) FEM can be higher than 25×. The accuracy is within round-off error compared to the standard FDM.

B. Open Resonator

A rapid plane solver has been described in [10] for the open resonator and the details are not repeated here. For this case, a 2-D discrete cosine transform can be used to obtain a rapid plane solver. This ensures that homogeneous Neumann boundary conditions are met along the boundaries of the resonator.

Both the shorted and open resonators are based on the 2-D Helmholtz equation (2); hence, their accuracy ultimately depend on the accuracy of this equation to model the resonators. For

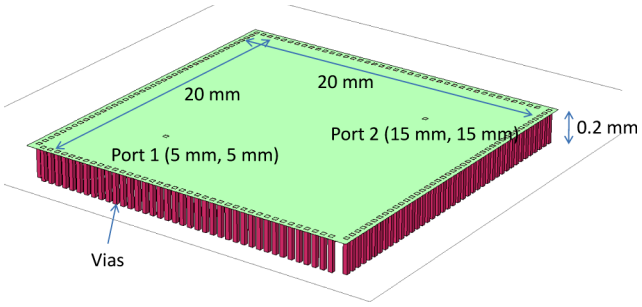

Fig. 5. Geometry of the shorted resonator simulated using Sonnet and the rapid plane solver.

very thin dielectrics, where the fringe effects are negligible, the 2-D Helmholtz equation is an excellent approximation as long as the wavelength is much smaller than the dielectric thickness. However, for typical dielectrics, there will be some fringe fields and radiation from the edge of the board for the open type resonator. The radiated fields are not included in (2); hence, the rapid plane solver for open resonators does not include radiated loss. For the shorted resonator, on the other hand, there is negligible radiation. Hence, if an electrical wall can be realized by using an excessive number of ground vias or by using conducting tape around the edges of the board, the losses in a shorted resonator can be more accurately modeled using the rapid plane solver compared to an open type resonator. This should increase the accuracy in extraction of dielectric losses.

To demonstrate the accuracy, an open resonator and a shorted resonator was simulated using both the rapid solver and a full-wave EM solver Sonnet.[1] The resonators had a square shape with a side length of 20 mm, $\varepsilon_r = 4$, $\tan\delta = 0.025$, dielectric thickness of 0.2 mm, and copper conductors with 35-μm thickness. For the shorted resonator, the two probes were located at locations (5 mm, 5 mm) and (15 mm, 15 mm), as shown in Fig. 5. Since the electric wall is realized using vias, the question arises as where to define the location of the electrical wall in the rapid plane solver. As this figure suggests, the distance between the inner edges of the planes were 20 mm in Sonnet simulation. A best match between the rapid solver and the Sonnet results were obtained when the electric wall was defined at the center of the vias in the rapid solver, which increased the plane size from 20 mm $\times$ 20 mm to 20.25 mm $\times$ 20.25 mm.

Fig. 6 shows the transfer impedance simulated using the rapid plane solver and Sonnet demonstrating good accuracy in both the magnitude and resonance frequency.

Next, an open resonator was simulated with the same properties as the shorted resonator, except that the ports were placed at two opposite corners of the resonators. Although the resonances match very well, the impedance peaks in the rapid plane solver are higher in magnitude compared to the full-wave simulation result obtained using Sonnet, as shown in Fig. 7. The reason is that the radiation losses are not included in the rapid plane solver. The accuracy of the extracted loss tangent would be higher than the actual value to compensate for this additional loss. Fig. 8 shows the loss factor calculated when the dielectric is lossless and conductors are perfect for the considered shorted and open resonators. The loss factor here corresponds to the radiation losses, which is the main source of discrepancy in the open resonator simulation in Fig. 7. For the shorted resonator, the radiation losses are negligible, as expected.

[1]Sonnet 11.56, Sonnet Software Inc., North Syracuse, NY.

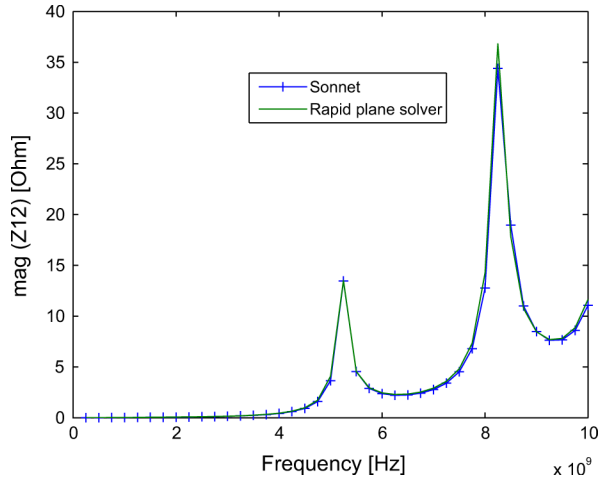

Fig. 6. Shorted resonator in Fig. 5 simulated using Sonnet and the rapid plane solver.

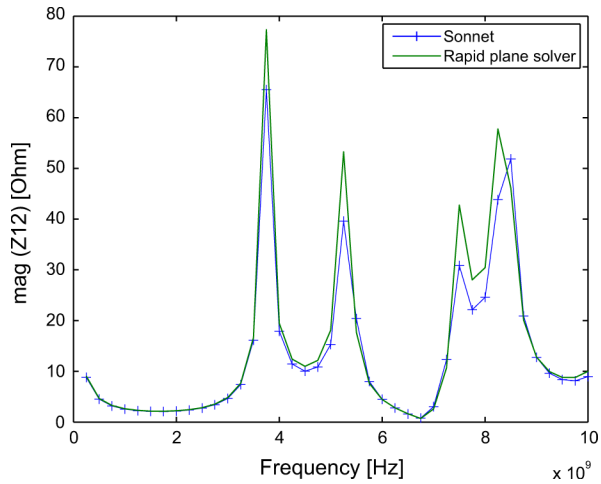

Fig. 7. Open resonator simulated using Sonnet and the rapid plane solver.

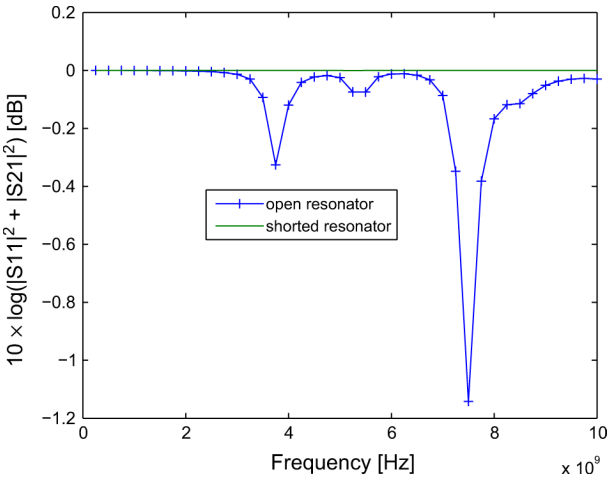

Fig. 8. Radiation loss factor for an open resonator simulated using Sonnet.

C. Incorporation of Losses

The finite-difference approximation of the Helmholtz equation (2) as obtained by the rapid plane solver can be considered as a bedspring model consisting of a 2-D array of per unit cell series inductances and shunt capacitances. Losses can be included in this model by using a complex permittivity and permeability function. The complex permittivity is defined in the usual way as

$$\varepsilon = \varepsilon'(1 - j\tan\delta) \tag{5}$$

where ε' is the real part of the permittivity and $\tan\delta$ is the loss tangent of the dielectric. The conductor losses can be approximated with the surface impedance as

$$R_s = 2\sqrt{\frac{j\omega\mu_c}{\sigma_c}}\coth\left(t\sqrt{j\omega\mu_c\sigma_c}\right) \tag{6}$$

where s is the Laplace variable, μ_c is the permeability of the conductors, σ_c is the conductivity of the conductors, and t is the thickness of the conductors [13]. The $coth$ function arises from the solution of a plane wave incident on a thin metal sheet and ensures the expected $\sqrt{f}$ variation of the skin-effect resistance, as well as the correct dc resistance value [14]. The surface impedance in (6) is a minimum-phase (hence, causal) function. To incorporate the conductor losses, a complex permeability for the dielectric can then be used as

$$\mu = \mu'\left(1 + \frac{R_s}{j\omega\mu' d}\right) \tag{7}$$

where μ' is the real part of the permeability of the dielectric, which is equal to the permeability of free space in most cases, and d is the thickness of the dielectric. This complex permeability changes the lossless per-unit-cell impedance of $j\omega\mu d$ to the correct lossy definition of $j\omega\mu' d + R_s$. A similar complex permeability has been used in [15] to incorporate conductor losses in modeling of planar structures in power distribution networks.

D. Probing Points

Measurements can be taken on the resonators using a vector network analyzer (VNA). Although coaxial cables of the VNA can be soldered on the resonator with appropriate connectors, using microprobes typically requires smaller probing pads increasing the accuracy of the measurement. For the open resonator structures, the probing can even be accomplished from the sides, which does not require any vias for the probing pads [16]. This is not possible for the shorted resonator type and vias must be drilled to connect the probes to the lower plate. At the resonance frequency, the open resonator has a voltage distribution of the form

$$V = V_0\cos\left(\frac{m\pi x}{a}\right)\cos\left(\frac{m\pi y}{b}\right) \tag{8}$$

corresponding to the TM_{mn0} mode of the open waveguide resonator. Similarly, the shorted resonator exhibits a voltage distribution of the form

$$V = V_0\sin\left(\frac{m\pi x}{a}\right)\sin\left(\frac{m\pi y}{b}\right) \tag{9}$$

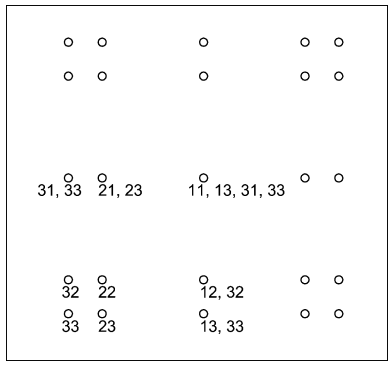

Fig. 9. Location of the impedance maxima up to the $m = 3$, $n = 3$ mode for the shorted resonator. For clarity, the corresponding modes for the maxima are shown only in the lower left quadrant, which repeats itself symmetrically in the other quadrants.

where V_0 is an arbitrary constant. In order to excite the resonances and pick up a large impedance magnitude, the probes should be placed at the maxima of these voltage profiles. For the open resonator, a good location is the corners of the resonator since the corners are at a maximum point of the cosine functions in both directions in (8). On the other hand, it is, of course, not possible to excite the shorted resonator by a probe on the edge. Fig. 9 shows the location of the maxima for the nine resonance modes up to TM_{330}. Note that, unlike the open resonator, TM_{0n0} or TM_{m00} modes do not exist for the shorted resonator. It is desirable to place the probes at locations where they are close to the maxima of the modes, as shown in Fig. 9, and far from the minima. For each considered mode, (9) can be evaluated to find the probe locations that correspond to an overall high voltage magnitude. Optimal points can be defined those that have the largest minimum value considering the various modes. Considering the nine resonance modes up to TM_{330}, some of the optimal locations lie 1/4 of the diagonal away from the corners of the plane. This actually corresponds to the location of the $(2, 2)$ mode maxima in Fig. 9.

To see the effect of the probe locations, two probes were placed 1/4, 1/5, and 1/6 of a diagonal away from opposite corners of the resonator. The considered shorted resonator has a dielectric constant of 4, loss tangent of 0.025, copper plates of 35-μm thickness, and a square shape of 2 cm on the side. Fig. 10 shows the magnitude of the transfer impedance, simulated using the rapid plane solver. Placing the two probes 1/4 of a diagonal away from two opposite corners resulted in higher impedance peaks for the first three resonances, which would result in greater measurement accuracy.

Finally, it is possible to choose a rectangular design instead of a square-shaped resonator to have distinct resonance frequencies for a TM_{mn0} and TM_{nm0} mode; however, it should be taken into account that the impedance peaks for the same resonance frequencies might also decrease for a rectangular design.

III. Characterization of a Low-Loss Substrate and FR-4

A. Extraction of Complex Permittivity

A standard FR-4 substrate and a low-loss substrate were characterized using shorted resonators of size 8 cm × 8 cm.

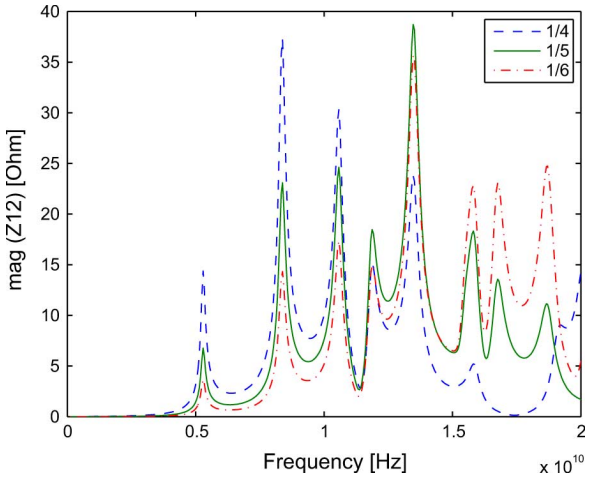

Fig. 10. Transfer impedance between two points located 1/4, 1/5, and 1/6 of a diagonal away from two opposite corners of a square-shaped shorted resonator.

The two ports were placed 1/4 of a diagonal away from two opposite corners of the resonator. The two-port S-parameters were measured using the VNA Agilent E5071C, and 250-μm ground–signal–ground (GSG) probes from Cascade. The measurements were taken after a short-open-load-thru (SOLT) calibration from 300 kHz to 20 GHz at 1601 linearly spaced frequency points. The transfer impedance was then obtained from the calibrated S-parameters and compared against rapid plane solver simulations to extract the loss tangent and dielectric constant at resonance frequency points, as shown in Fig. 11. In the simulations, a discretization of 512 unit cells in each direction was used, resulting in a mesh length of less than 0.1 mm. The dielectric thickness was obtained as 193 μm to get the best match between simulations and measurements. Even though this method allows to extract the dielectric thickness, it is also possible to measure the dielectric thickness from the cross section very accurately to simplify the fitting procedure. For each subfigure, a different dielectric constant and loss tangent has been used in the simulator. In fitting these parameters, it is useful to consider the locations of the resonances for extracting the dielectric constant, whereas the peak amplitudes are mostly sensitive to the loss tangent.

The results for the low-loss substrate are shown in Fig. 12. The dielectric thickness in this case was obtained as 188 μm. As expected, the resonances are sharper compared to the more lossy FR-4 substrate in Fig. 11 since the loss tangent is much smaller. In both cases, the simulations match measurements very well around all resonance points. Note that the resonance frequencies chosen in Figs. 11 and 12 do not necessarily correspond to the same modes.

B. Modeling of Complex Permittivity

Figs. 11 and 12 show that the extracted material properties are frequency dependent. Any model for complex permittivity should satisfy the Kramers–Kronig relation; otherwise, the resulting model would be noncausal and provide inaccurate results in time-domain simulation [17]–[19].

When resonators are used for extraction of material properties, data is obtained at discrete frequency points. Extrapolation of the data would be needed to estimate the material properties

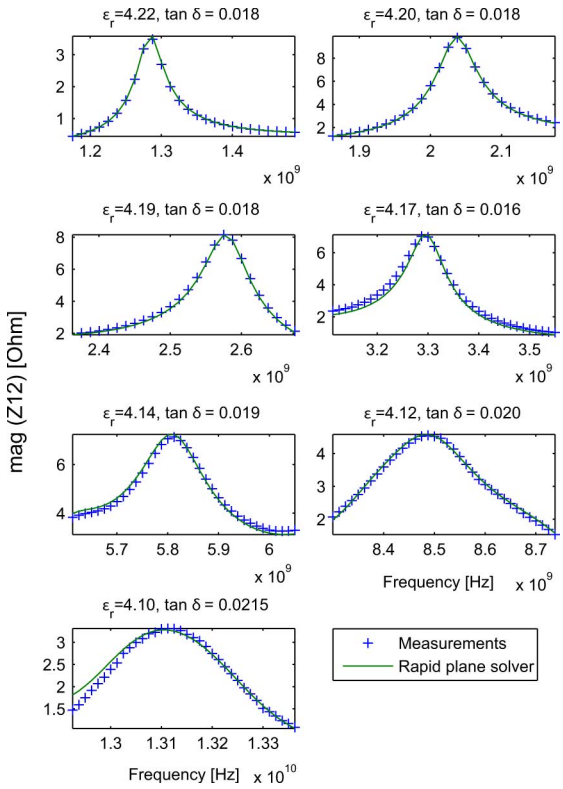

Fig. 11. Standard FR-4 substrate: measurement results versus rapid plane solver for a 8 cm × 8 cm shorted resonator at various resonance frequency points.

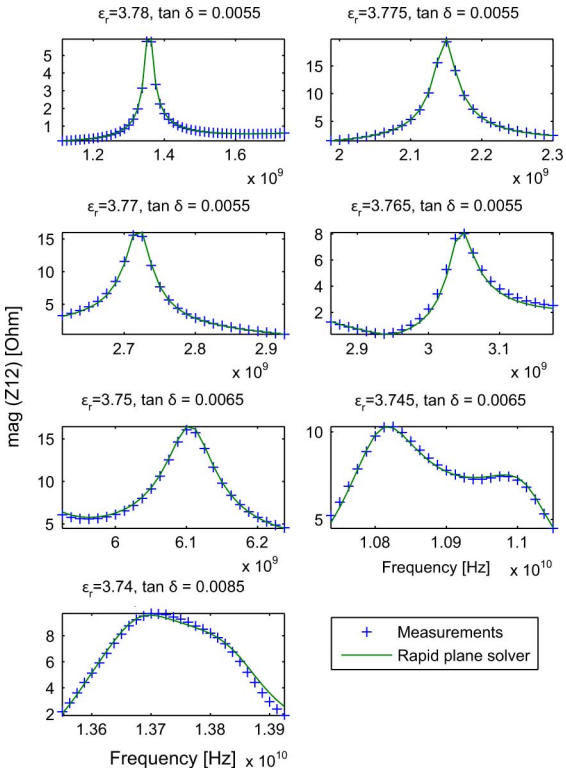

Fig. 12. Low-loss substrate: measurement results versus rapid plane solver for a 8 cm × 8 cm shorted resonator at various resonance frequency points.

outside the frequency range of the resonances of the structures. This is required, for example, to analyze the dispersion and attenuation of digital signals, which are broadband in nature.

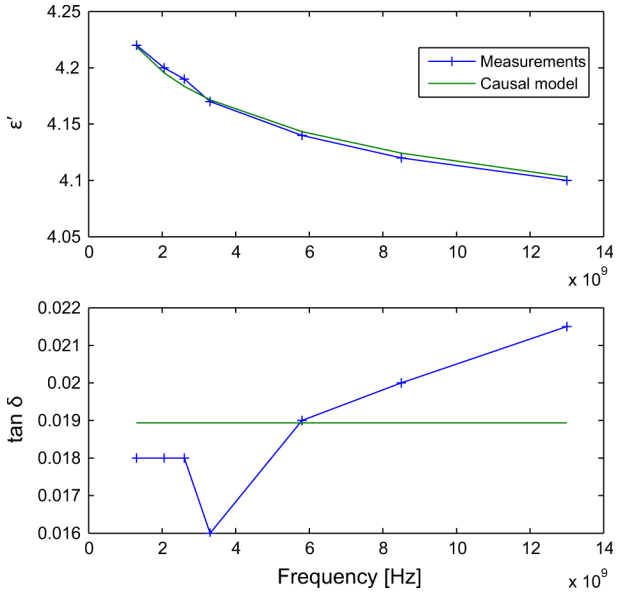

Fig. 13. Standard FR-4 substrate: comparison of the dielectric constant and loss tangent extracted from measurements versus constant-phase causal model.

When extrapolating the data, it is useful to consider that commonly used PCB substrates such as FR-4 tend to have an approximately constant loss tangent in the frequency range of interest [6], [19]. For this purpose, an average loss tangent value can be used to obtain a simple broadband model for such dielectrics. A constant loss tangent, however, implies that the dielectric constant is frequency dependent according to Kramers–Kronig relation. Actually, since the complex permittivity is a minimum-phase function, the dielectric constant can be exactly defined (up to a constant) for a given frequency-independent loss tangent using the equation

$$\varepsilon = as^{-2\delta/\pi} \tag{10}$$

where a is an arbitrary positive constant, δ is the argument of $\tan\delta$, and s is the Laplace variable [14], [20]. This constant-phase function has been fitted to the extracted dielectric constant and loss tangent shown in Fig. 11. The result shown in Fig. 13 indicates a good fit of the function to the extracted data.

Note how the constant-phase function in (10) results in a constant loss tangent, as shown in Fig. 13, whereas the frequency-dependent behavior of the dielectric constant is captured very well. Next, the obtained constant-phase function is used in the rapid plane solver to incorporate the frequency-dependent complex permittivity function. The comparison with measurement results is shown in Fig. 14, indicating good accuracy in both the location of the resonances, as well as the amplitudes of the impedance peaks.

The constant-phase function has been fitted to the data shown in Fig. 12 for the low-loss substrate as well. The comparison of the extracted data versus the fitted model is shown in Fig. 15. The extracted loss tangent in this case is about 1/3 of the FR-4 substrate, demonstrating the capability of the presented approach to characterize low-loss substrates as well.

The comparison of the simulation data using the constant-phase model for the complex permittivity versus the measurements is shown in Fig. 16. A very good agreement can be observed between the results.

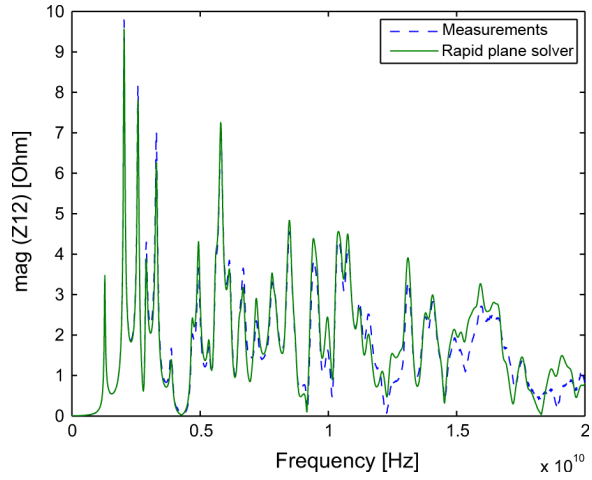

Fig. 14. Standard FR-4 substrate: comparison of simulation versus measurements.

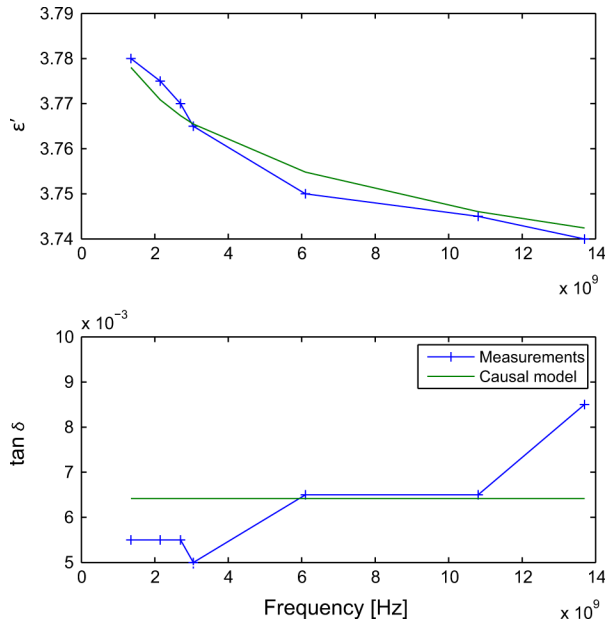

Fig. 15. Low-loss substrate: comparison of the dielectric constant and loss tangent extracted from measurements versus constant-phase causal model.

IV. Analytical Debye Modeling of Substrates With Constant Loss Tangent

For PCB dielectrics, the complex permittivity can be approximated using a Debye model as

$$\varepsilon(s) = \varepsilon'_\infty + \sum_{i=1}^{K} \frac{a_i}{1+s\tau_i} \tag{11}$$

where a_i and τ_i represent the strength and time constants of various relaxation processes, and s is the Laplace variable. The order of the approximation K can be chosen as high as possible as long as the extracted a_i and τ_i are all positive and real numbers. The Debye model is quite useful in time-domain simulations, as it allows the consideration of the frequency-dependent material properties using an *RC* type of an equivalent-circuit model in SPICE or FDTD solvers. One example is shown in

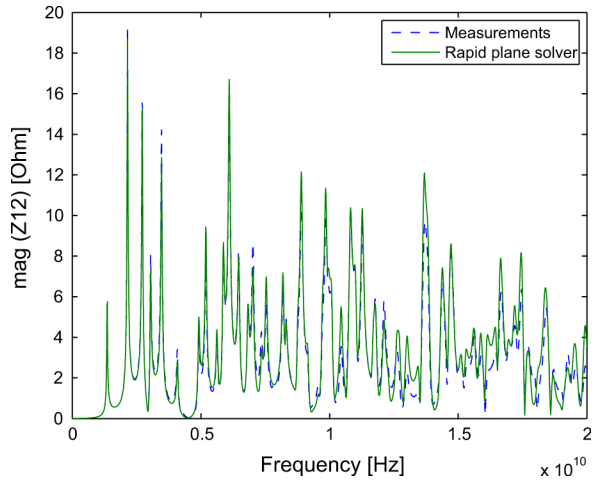

Fig. 16. Low-loss substrate: comparison of simulation versus measurements.

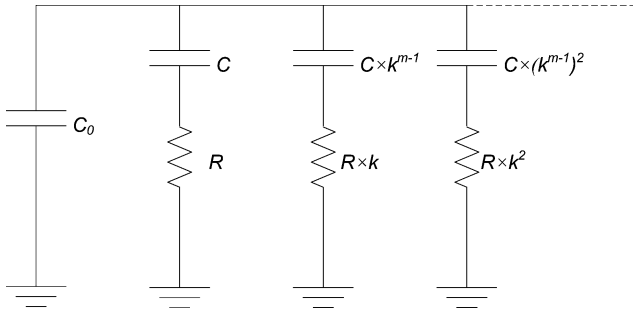

Fig. 17. Debye model of a lossy capacitor with a constant loss tangent.

Fig. 17, where the Debye model in (11) has been used to model a lossy capacitor with a constant loss tangent. Based on (10), the admittance of such a network is given by

$$Y = s\frac{\varepsilon}{\varepsilon_{\text{air}}}C_{\text{air}} = \frac{C_{\text{air}}}{\varepsilon_{\text{air}}}as^{1-2\delta/\pi} \tag{12}$$

where the subscript air refers to the permittivity or the capacitance calculated when the medium is replaced with free space. The Debye model in Fig. 17 can then be considered as an approximation of this admittance.

Even though the vector-fitting algorithm [21] could be used to obtain a rational function approximating (12), it cannot be guaranteed that the resulting circuit would be of an *RC* type, as shown in Fig. 17. On the other hand, for the case of a complex permittivity described by a constant-phase function, as in (12), a simpler model can be generated analytically without requiring any curve fitting. The model shown in Fig. 17 for this purpose has been used before in realization of general *RC* constant-argument driving-point admittances [22].

To adapt the approach in [22] to a lossy capacitor described by a Debye model, the following parameters should be provided:

- C_0: high-frequency asymptote of the capacitance;
- ω_0: upper frequency bound for the validity of the model;
- $\tan\delta$: loss tangent;
- k: spacing factor to be chosen based on the required accuracy versus bandwidth of the model;
- N: number of *RC* branches.

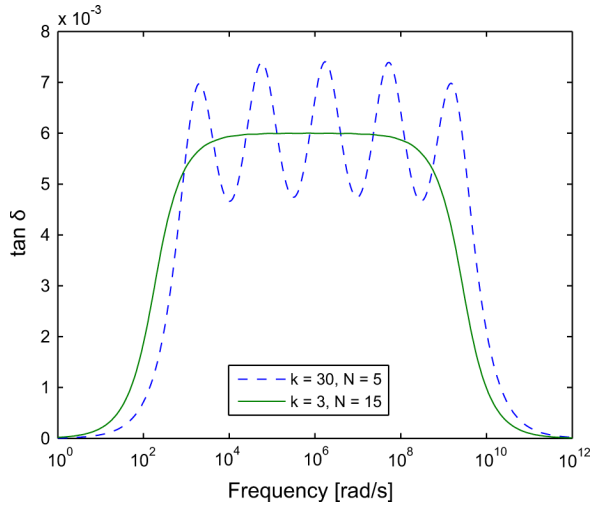

Fig. 18. Loss tangent approximated using the Debye model for the example of $C_0 = 10^{-12}$ F, $\omega_0 = 10^{10}$ rad/s, and $\tan\delta = 0.006$.

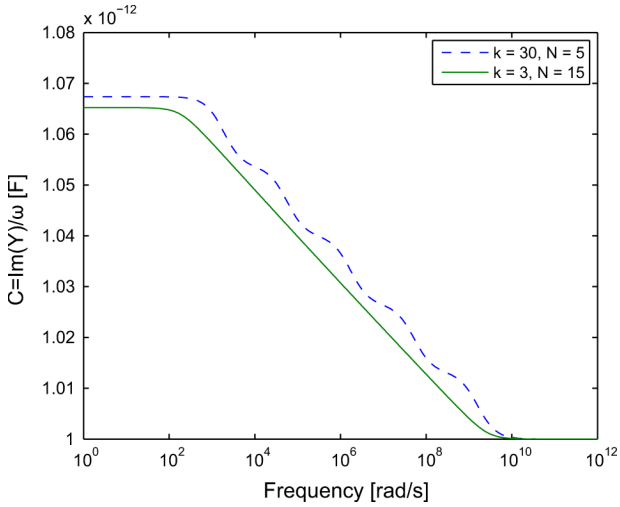

Fig. 19. Capacitance approximated using the Debye model for the example of $C_0 = 10^{-12}$ F, $\omega_0 = 10^{10}$ rad/s, and $\tan\delta = 0.006$.

Based on this input, the values of the circuit elements in Fig. 17 can be obtained analytically following [22] as

$$m = \frac{1}{1-\frac{2\delta}{\pi}} \tag{13}$$

$$C = C_0(k^{m-1}-1) \tag{14}$$

$$R = \frac{1}{w_0 C}. \tag{15}$$

As the number of *RC* branches N in this network is increased, the lower frequency bound for the validity of the model decreases, which results in increased bandwidth of the model. To demonstrate the approach, consider the example with the given parameters of $C_0 = 10^{-12}$ F, $\omega_0 = 10^{10}$ rad/s, and $\tan\delta = 0.006$.

Fig. 18 shows the performance of the presented Debye model to represent a constant loss tangent. The spacing factor k can be increased to use a lesser number of branches in the model. The tradeoff is the increased sinusoidal variation around the desired loss tangent, decreasing the accuracy of the model. By using a

small k and sufficient number of branches, perfect approximation of a constant loss tangent in the desired frequency range is possible, as demonstrated in this figure. Note that a very accurate model for a bandwidth of 4–5 decades was obtained using 15 branches in this example.

Fig. 19 shows the variation of the capacitance with frequency. As expected, the capacitance approaches the high-frequency asymptote C_0 at frequencies higher than ω_0. At very low frequencies, the capacitance also approaches the parallel connection of all the capacitors in the model.

V. Conclusion

This paper has presented a new approach for characterization and modeling of the dielectric constant and loss tangent of substrates used in chip packages and PCBs.

The extraction of the material properties is achieved by taking measurements on a simple shorted waveguide resonator. Due to the simple geometry of this resonator, it is possible to simulate it very efficiently. In this paper, a rapid plane solver for a shorted resonator has been introduced for the first time. Using this simulator, the dielectric constant and loss tangent is extracted by overlapping the measurement results with simulation results. Since this procedure involves iteratively adjusting the dielectric constant and loss tangent in the simulator, the efficiency of the presented simulator becomes very useful. A problem size of five million unknowns was simulated within 30 s on a PC with a 1.4-GHz clock frequency.

Measurements were taken on FR-4 and a low-loss substrate to test the method. The extracted dielectric constant and loss tangent were then fitted to a Debye model. For the first time, a method has been presented that analytically generates a broadband Debye model. Independent of the method used to extract the material properties, this new method of generating a Debye model can be used on any substrate that exhibits an approximately constant loss tangent, which is true for most dielectrics used in PCBs and chip packages. A broad frequency range can be modeled using a small number of circuit elements, making this approach very attractive for time-domain simulation of lossy interconnects, transmission lines, and power/ground planes in circuit simulators or FDTD type of solvers.

References

[1] A. Deutsch, T.-M. Winkel, G. Kopcsay, C. Surovic, B. Rubin, G. Katopis, B. Chamberlin, and R. Krabbenhoft, "Extraction of $\varepsilon_r(f)$ and $\tan\delta(f)$ for printed circuit board insulators up to 30 GHz using the short-pulse propagation technique," *IEEE Trans. Adv. Packag.*, vol. 28, no. 1, pp. 4 –12, Feb. 2005.

[2] S. Yamacli, C. Ozdemir, and A. Akdagli, "A method for determining the dielectric constant of microwave PCB substrates," *Int. J. Infrared Millim. Waves*, vol. 29, no. 2 , pp. 207–216, Feb. 2008.

[3] X. Fang, D. Linton, C. Walker, and B. Collins, "Dielectric constant characterization using a numerical method for the microstrip ring resonator," *Microw. Opt. Technol. Lett.*, vol. 41, no. 1 , pp. 14–17, Apr. 2004.

[4] J.-M. Heinola and K. Tolsa, "Dielectric characterization of printed wiring board materials using ring resonator techniques: A comparison of calculation models," *IEEE Trans. Dielect. Elect. Insulation*, vol. 13, no. 4 , pp. 717–726, Aug. 2006.

[5] R. K. Hoffmann, *Handbook of Microwave Integrated Circuits*. Norwood, MA: Artech House, 1987.

[6] A. Djordjevic, R. Biljie, V. Likar-Smiljanic, and T. Sarkar, "Wideband frequency-domain characterization of FR-4 and time-domain causality," *IEEE Trans. Electromagn. Compat.*, vol. 43, no. 4 , pp. 662–667, Nov. 2001.

[7] *Non-Destructive Full Sheet Resonance Test for Permittivity of Clad Laminates*, IIPEC Standard IPC-TM-650, 2.5.5.6, May 1989.

[8] A. Deutsch, A. Huber, G. Kopcsay, B. Rubin, R. Hemedinger, D. Carey, W. Becker, T.-M. Winkel, and B. Chamberlin, "Accuracy of dielectric constant measurement using the full-sheet-resonance technique IPC-TM-650 2.5.5.6," *Electr. Perform. Electron. Packag.*, pp. 311–314, 2002.

[9] N. Biunno and I. Novak, "Frequency domain analysis and electrical properties test method for PCB dielectric core materials," presented at the DesignCon 2003 East, Boston, MA, Jun. 2003.

[10] A. E. Engin, A. Tambawala, M. Swaminathan, P. Pramanik, and K. Yamazaki, "Causal modeling and extraction of dielectric constant and loss tangent for thin dielectrics," in *IEEE Int. Electromagn. Compat. Symp.*, Honolulu, HI, Jul. 2007, pp. 1–5.

[11] J. Howell, "A quick accurate method to measure the dielectric constant of microwave integrated-circuit substrates," *IEEE Trans. Microw. Theory Tech.*, vol. MTT-21, no. 3 , pp. 142–144, Mar. 1973.

[12] G. Strang, *Introduction to Applied Mathematics*. Cambridge, MA: Wellesley–Cambridge Press, 1986, pp. 453–458.

[13] L. Giacoletto, "Frequency- and time-domain analysis of skin effects," *IEEE Trans. Magn.*, vol. 32, no. 1 , pp. 220–229, Jan. 1996.

[14] A. E. Engin, W. Mathis, W. John, G. Sommer, and H. Reichl, "Closed-form network representations of frequency-dependent $RLGC$ parameters," *Int. J. Circuit Theory Appl.*, vol. 33, pp. 463–485, Nov. 2005.

[15] V. Kollia and A. Cangellaris, "A methodology for incorporating metallization loss in the electromagnetic modeling of the power distribution network," in *IEEE Elect. Perform. Electron. Packag.*, Oct. 2008, pp. 343–346.

[16] J. R. Miller, G. Blando, K. B. A. Williams, and I. Novak, "Impact of PCB laminate parameters on suppressing modal resonances," presented at the DesignCon, Feb. 2008.

[17] T. Arabi, A. Murphy, T. Sarkar, R. Harrington, and A. Djordjevic, "On the modeling of conductor and substrate losses in multiconductor, multidielectric transmission line systems," *IEEE Trans. Microw. Theory Tech.*, vol. 39, no. 7 , pp. 1090–1097, Jul. 1991.

[18] C. Morgan, "Solutions for causal modeling and a technique for measuring causal, broadband dielectric properties," presented at the DesignCon, Feb. 2008.

[19] C. Svensson and G. Dermer, "Time domain modeling of lossy interconnects," *IEEE Trans. Adv. Packag.*, vol. 24, no. 2 , pp. 191–196, May 2001.

[20] H. W. Johnson and M. Graham, *High-Speed Signal Propagation: Advanced Black Magic*. Upper Saddle River, NJ: Prentice-Hall, 2003.

[21] B. Gustavsen and A. Semlyen, "Rational approximation of frequency domain responses by vector fitting," *IEEE Trans. Power Del.*, vol. 14, no. 3, pp. 1052–1061, Jul. 1999.

[22] R. Morrison, "*RC* constant-argument driving-point admittances," *IRE Trans. Circuit Theory*, vol. CT-6 , no. 3 , pp. 310–317, Sep. 1959.

A. Ege Engin (M'05) received the B.S. degree in electrical engineering from Middle East Technical University, Ankara, Turkey, in 1998, the M.S. degree in electrical engineering from the University of Paderborn, Paderborn, Germany in 1998, and the Ph.D degree (*summa cum laude*) from the University of Hannover, Hannover, Germany, in 2004.

He was a Research Engineer with the Fraunhofer-Institute for Reliability and Microintegration, Berlin, Germany. From 2006 to 2008, he was an Assistant Research Director with the Microsystems Packaging Research Center, Georgia Institute of Technology. He is currently an Assistant Professor with the Department of Electrical and Computer Engineering, San Diego State University, San Diego, CA. He has authored or coauthored over 70 publications in journals and conferences in the areas of signal and power integrity modeling and simulation. He holds one patent with three pending. He coauthored *Power Integrity Modeling and Design for Semiconductors and Systems* (Prentice-Hall, 2007).

Dr. Engin was the recipient of the 2009 Semiconductor Research Corporation Inventor Recognition Award. He coauthored publications that received the Outstanding Poster Paper Award at the 2006 Electronic Components and Technology Conference (ECTC) and the Best Paper of the Session Award of the 2007 International Microelectronics And Packaging Society (IMAPS). He was a Best Paper Award finalist in the Board-Level Design Category, DesignCon 2007.